



The dielectric and magnetic properties of RTV-silicon rubber Ni–Cr ferrite composites

O. M. Hemeda¹ · A. M. A. Henaish^{1,2} · B. I. Salem¹ · F. S. El-Sbakhly^{1,3} · Mahmoud A. Hamad⁴

Received: 28 August 2019 / Accepted: 7 January 2020 / Published online: 22 January 2020
© Springer-Verlag GmbH Germany, part of Springer Nature 2020

Abstract

In this work, polymeric composites based on room-temperature vulcanized (RTV) silicon rubber incorporated with different $\text{NiCr}_{0.2}\text{Fe}_{1.8}\text{O}_4$ (NCF) content are prepared. The results indicate the well dispersion of various micron-sized particles of NCF with low agglomerations. The decrease in the density is the most advantage property that allows us to obtain the light magnetic material for industrial applications. It is shown that the rubber occupies the porous and defects between NCF particles. It is found that dielectric constant is enhanced with RTV content and decreases with increasing selected frequency for all samples. The electrical conductivity of composite is enhanced with both RTV content and the heat treatment temperature of composites. The saturation magnetization is strongly dependent on NCF content in RTV matrix.

Keywords Ni–Cr ferrites · RTV-silicon rubber · XRD · Dielectric constant · Magnetic properties

1 Introduction

The advantages of polymeric composite materials have superiority over metallic and ceramic materials [1–11]. Ferrite is considered one of the most important magnetic materials and cannot be replaced by other materials because of its low cost and chemical stability and low eddy current losses [12–15]. Therefore, the ferrites are widely used in many applications, although they are less magnetic performance than rare materials. The ferrite in the form of ceramic is used as a component in multi-devices such as noise filters, magnetic storage, transformer cores, circulators, refrigerators, radio, and TV, and in other devices [16–20]. Among these ferrites, NiFe_2O_4 ferrites are of great interest due to their significant properties such as low cost-effectiveness, chemical stability, highly permeability at highly frequency,

and large electrical resistivity [21]. The structure of NiFe_2O_4 belongs to inverse spinel structure, where half of the B sites are occupied by Ni^{2+} ions, while the other half on B sites are occupied by Fe^{3+} ions in the same time the half of the Fe^{3+} ions rest on A sites [22]. When NiFe_2O_4 ferrites are doped by chromium, the magnetic parameters like remanent magnetization (M_r), saturation magnetization (M_s), and coercive field (H_C) are tailored according to chromium content [23]. This chromium doping induces magnetic changing in this system and leads to tailor magnetic properties, due to chromium ion strongly prefers to occupy in the B-site, making antiferromagnetic coupling with Fe ion [24]. It is recommended the bulk NiFeCrO_4 sample to use as a permanent magnet, due to its high H_C [24]. Furthermore, compensation of the magnetic moments of the A and B sublattices for certain Cr content samples ordered antiferromagnetically in the ground state at low temperatures [25]. In addition, there are many effects which were observed in this system, such as Hall effect, magnetocaloric effect, magnetoresistance, and magneto-optical Faraday effect [26, 27]. Patange et. al have observed that lattice constant of $\text{NiFe}_{2-x}\text{Cr}_x\text{O}_4$ increases slightly with low chromium content up to $x=0.2$ due to the fact that up to 0.2 substitution of Cr^{3+} ions does not affect the lattice constant [28]. On the other hand, the conductive rubber is a material used to prevent the occurrence of wave interference and it is taken into account for a long period [29, 30]. There are many types of rubber used

✉ Mahmoud A. Hamad
m_hamad76@yahoo.com

¹ Physics Department, Faculty of Science, Tanta University, Tanta, Egypt

² NANOTECH Center, Ural Federal University, 620002 Yekaterinburg, Russia

³ Physics Department, Faculty of Engineering, Sinai University, El-Arish, Egypt

⁴ Basic Science Department, Higher Institute of Engineering & Technology, King Marriott Academy, Alexandria, Egypt

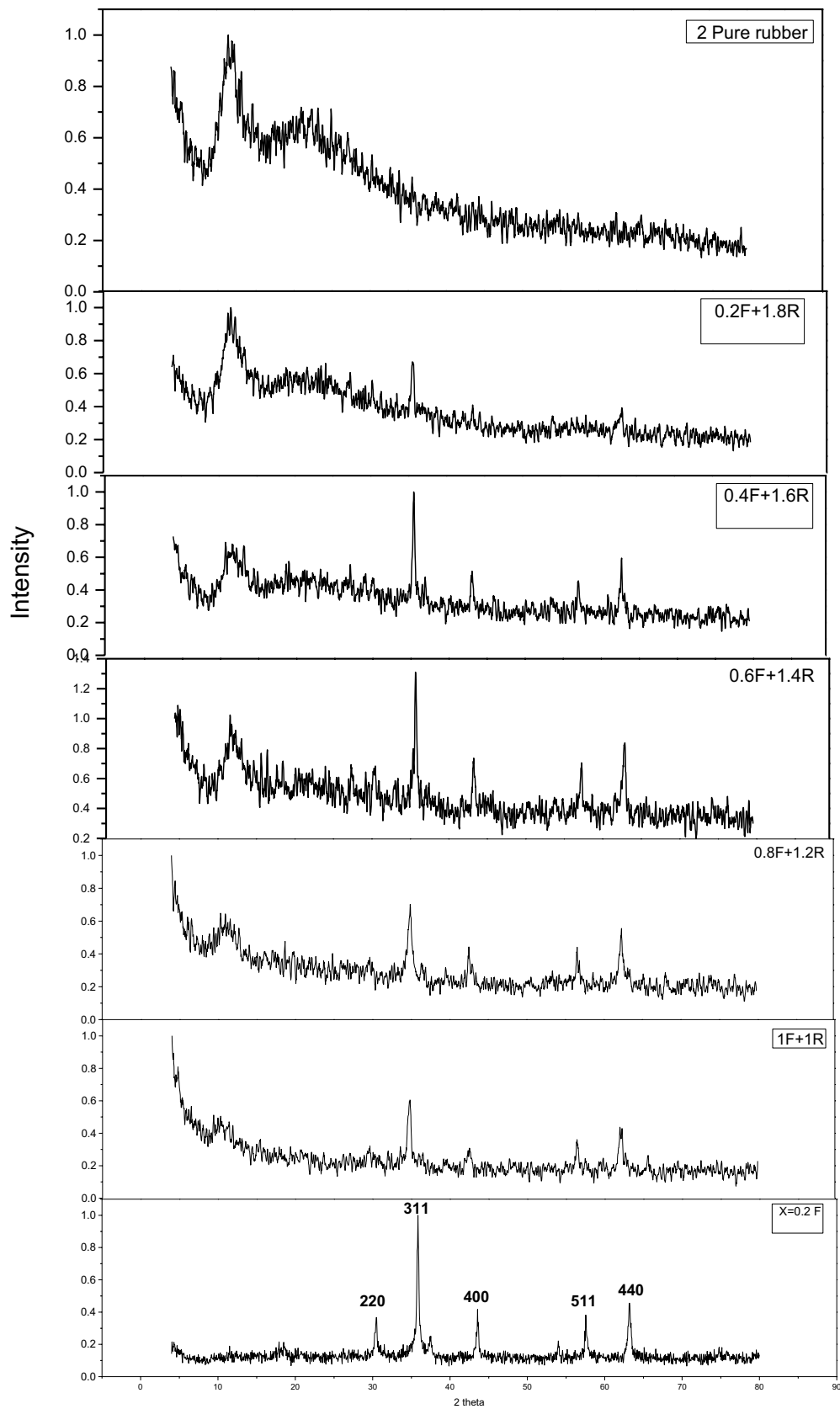
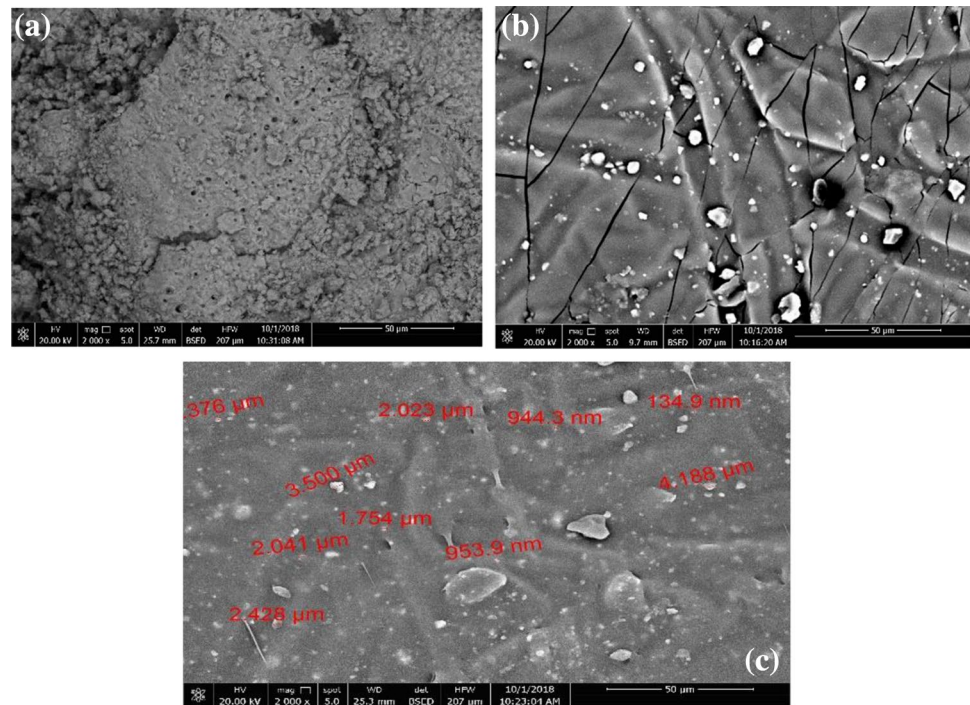


Fig. 1 XRD patterns of pure NCF and NCF-RTV-silicon rubber composites

Table 1 Values of lattice parameter, average crystallite size, X-ray density, and bulk density for pure NCF and NCF–RTV-silicon rubber composites

Composition	Lattice parameter a (Å)	Average crystallite size d (nm)	X-ray density D_x (g/cm ³)	Bulk density D_b (g/cm ³)
NCF	8.288	19.460	5.4523	5.310
NCF–RTV-silicon rubber	8.410	20.080	5.2170	1.5005
0.8 NCF + 1.2 RTV-silicon rubber	8.340	23.209	5.3509	1.3609
0.6 NCF + 1.4 RTV-silicon rubber	8.361	25.110	5.3099	1.2290
0.4 NCF + 1.6 RTV-silicon rubber	8.323	26.714	5.3823	1.1670
0.2 NCF + 1.8 RTV-silicon rubber	8.336	30.497	5.3577	0.999

Fig. 2 SEM micrograph of **a** pure NCF, **b** pure RTV-silicon rubber, and **c** NCF–RTV-silicon rubber composite

as conductive rubber such as silicon rubber, natural rubber, nitrile rubber, and so on [31]. One of these types, room-temperature vulcanized (RTV) silicon rubber is considered one of the best because of its resistance to corrosion, thermal stability, resistance to climate, and low surface tension [32–34]. To improve the properties of rubber composites, the thermal treatment is used at a certain temperature, called curing temperature, since some of the rubber characteristics can be cured at a large temperature range. Therefore, these features of $\text{NiCr}_{0.2}\text{Fe}_{1.8}\text{O}_4$ (NCF) and RTV motivate us to investigate the polymeric composites based on RTV-silicon rubber incorporated with different NCF content. The main aim of this work is to study the effect of incorporation of different NCF ferrite contents on RTV-silicon rubber matrix, and to correlate between electrical properties and curing temperature.

2 Experimental details

NCF powder with the chemical formula $\text{NiCr}_{0.2}\text{Fe}_{1.8}\text{O}_4$ was prepared by flash autocombustion method [35].

The prepared powder was then sintered at 400 °C for 2 h. RTV-silicon rubber matrix was incorporated into the pre-characterized powder samples according to the following ratios 0.8 NCF + 1.2 RTV, 0.6 NCF + 1.4 RTV, 0.4 NCF + 1.6 RTV, and 0.2 NCF + 1.8 RTV. This was then homogenized using a two-roll mixing mill. The composite samples were molded into thin disks with 2 mm thickness and 16 mm diameter. Philips model (PW-1729) diffractometer was used to investigate the structure properties of prepared samples, using X-ray diffraction (XRD). The average crystallite size was estimated from the most intense peaks of the XRD pattern of the samples using Scherer's equation [36, 37]:

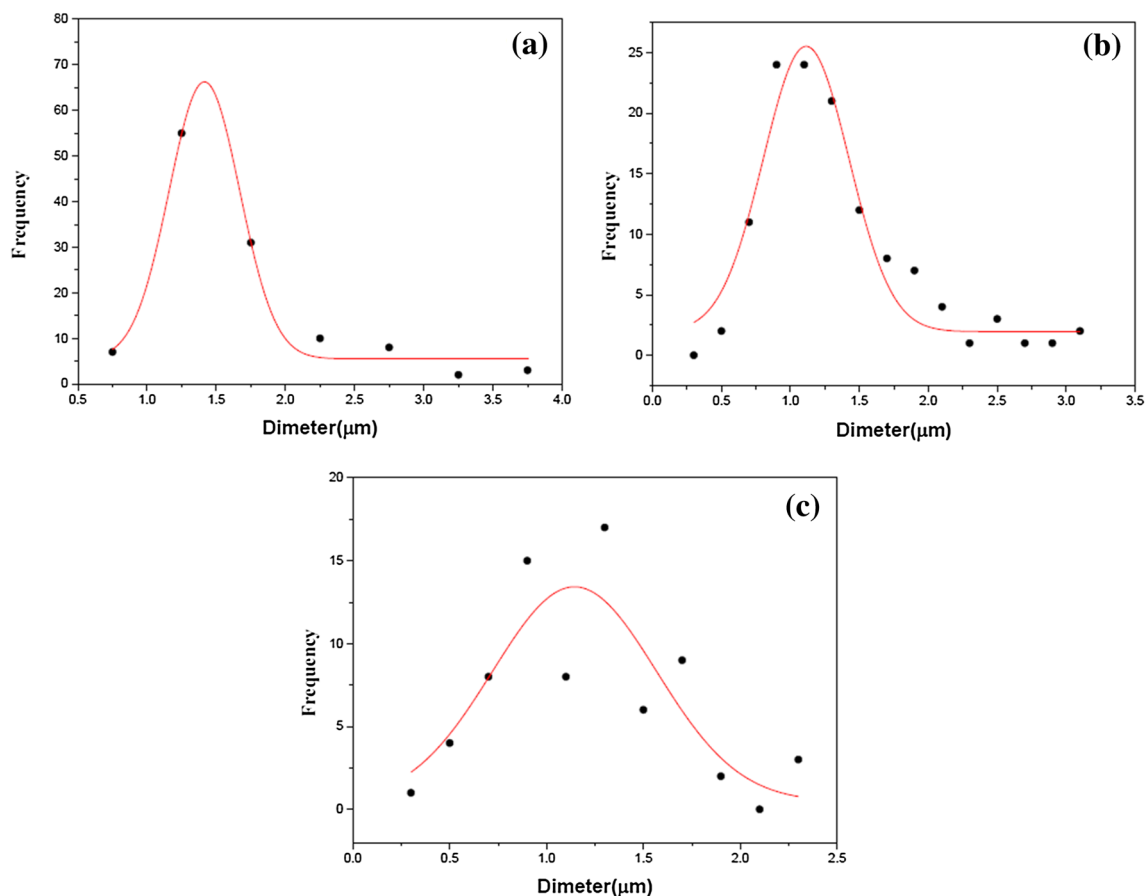


Fig. 3 Grain size distribution graphs of a pure NCF, b pure RTV-silicon rubber, and c NCF-RTV-silicon rubber composite

$$d = \frac{k\lambda}{\beta \cos\theta_B}, \tag{1}$$

where $k = 0.89$, β is the full width at half maximum, and θ_B is the diffraction angle. JEOL JSM-5600 Scanning Electron Microscope (SEM) was used to investigate the morphology. The dielectric constant (ϵ') and AC resistivity (ρ_{ac}) for prepared samples were measured using RLC Bridge-type MC2811C. The magnetic hysteresis loops of samples were recorded at room temperature by vibrating sample magnetometer model (Lakeshore 7304).

3 Results and discussion

3.1 X-ray diffraction analysis

To investigate the structure of NCF-RTV-silicon rubber composites, XRD measurements of pure silicon rubber, NCF, and NCF containing different silicon rubber content composite samples are shown in (Fig. 1). XRD patterns of NCF-RTV-silicon rubber composites were recorded from

2θ (4° – 80°) and the structure parameters of the composite samples were estimated. Comparing the structure parameters of the composite samples from the XRD pattern with the pure NCF reveals that the structure of NCF does not change during the stages of processing the rubber composite. The broad diffraction peak located at $2\theta = 11.56^\circ$ is attributed to the diffraction of RTV-silicon rubber, indicating that there exists a certain degree of ordered structure that usually accompanied by an internal partial regularity of RTV. Besides, with increasing content of NCF, the diffraction peak located at 11.62° became broader, revealing that NCF dispersed uniformly in the RTV-silicon rubber matrix with no large agglomeration or stack structure. It is suggested that NCF structure has good compatibility with RTV-silicon rubber. This could improve the interfacial interactions between NCF and RTV-silicon rubber. Furthermore, the average crystallite size of RTV-silicon rubber increases with ferrite due to the increase of internal stress. On the other hand, the XRD pattern of NCF ferrite demonstrates the cubic spinel structure and is indexed to (220), (311), (400), (511), and (440) crystal planes at $2\theta = 30.54^\circ$, 35.94° , 43.66° , 57.67° , and 63.30° , respectively, for cubic spinel

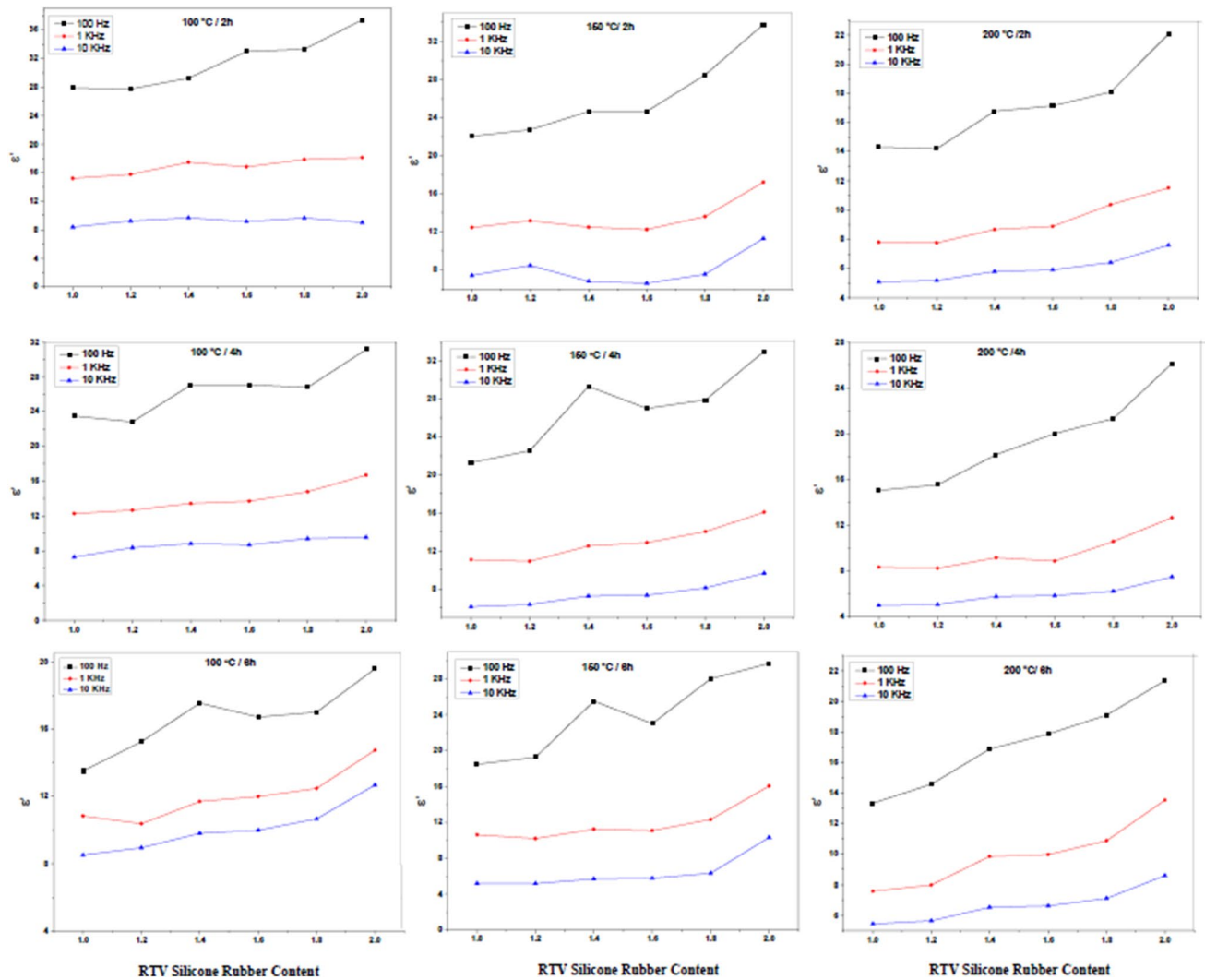


Fig. 4 ϵ'' as function of RTV content at selected frequencies 100 Hz, 1 kHz, and 10 kHz for composite samples that exposed to heat treatment at 100 °C, 150 °C, and 200 °C during different curing time 2, 4, and 6 h

phase with lattice parameter $a = 8.288 \text{ \AA}$. In addition, no impurity phases were detected. Furthermore, the relative intensity of peaks decreases with increasing RTV content, indicating the decrease of the degree of crystallinity of NCF ferrite. Moreover, the structure of NCF in all RTV-silicon rubber content composite samples is maintained. As shown in Table 1, there was a slight change in lattice parameter (a) and X-ray density. Furthermore, the bulk density of the composite samples decreases with RTV-silicon rubber. This decrease is the most advantage property that allows us to obtain the light magnetic material for industrial applications. However, Table 1 shows the average crystallite size of NCF ferrite in the composite samples increases with RTV-silicon rubber. This may be due to the accumulation of rubber in the grain boundaries of NCF ferrite phase, causing a change in internal stress, leading to lower the lattice parameters.

3.2 Morphology study of composites

Figure 2 shows SEM images of pure NCF, pure RTV-silicon rubber, and NCF–RTV-silicon rubber composite. The results of SEM indicate that the dispersion of various micron-sized particles of NCF (bright grains) with low agglomerations, forming irregular shapes in the RTV-silicon rubbers.

The grain size distributions of pure NCF, pure RTV-silicon rubber, and NCF–RTV-silicon rubber composite are given in Fig. 3. The results showed that mean grain sizes of the pure NCF and pure RTV-silicon rubber close to 1.5 and 1 μm with narrow distributions, as shown in Fig. 3a, b, respectively. However in NCF–RTV-silicon rubber composite, the grain size distribution showed broader distributions as shown in Fig. 3c, showing that the large grain size increases after incorporation NCF in RTV-silicon rubber matrix.

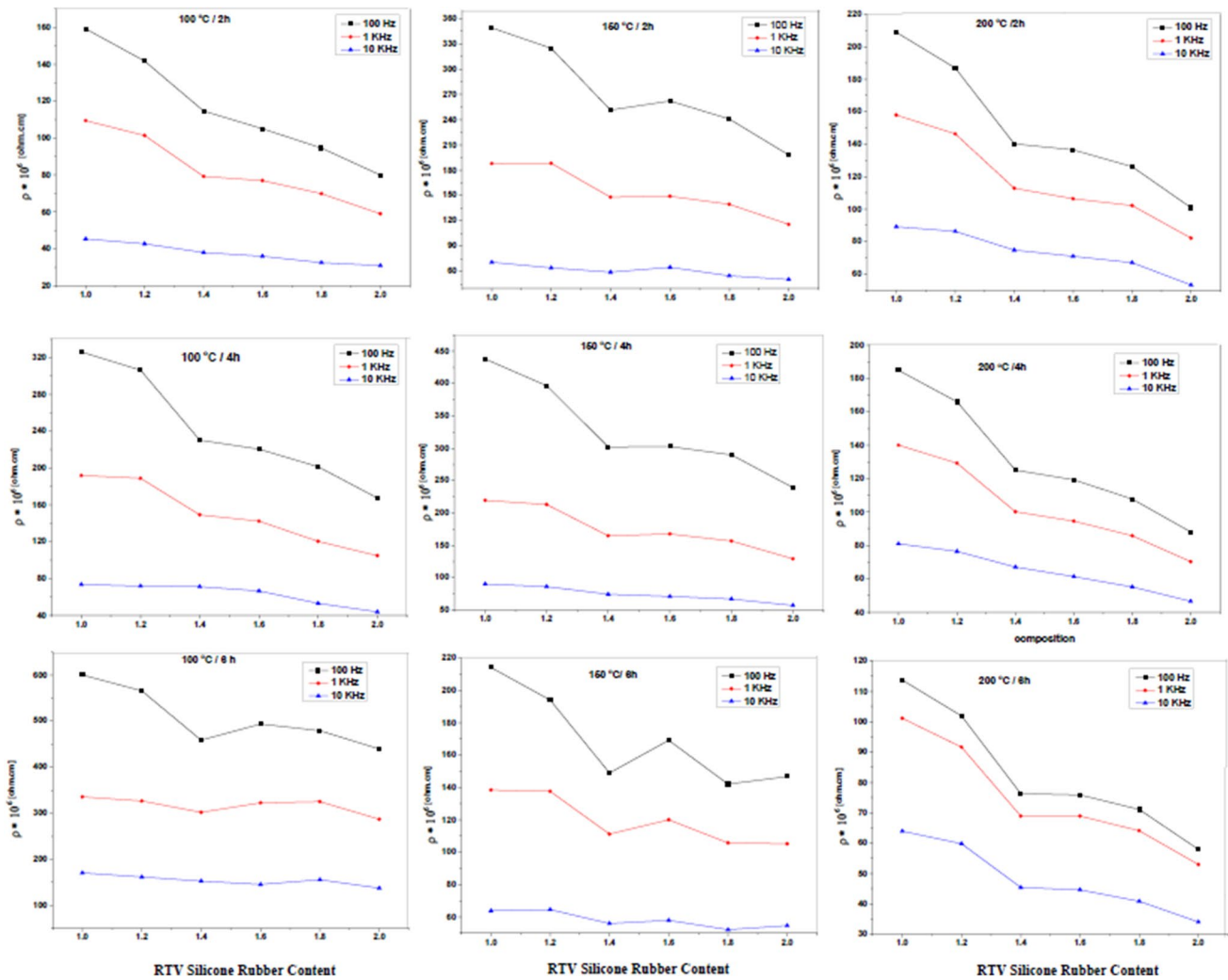


Fig. 5 ρ_{ac} as function of RTV-silicon rubber content at selected frequencies 100 Hz, 1 kHz, and 10 kHz for composite samples that exposed to heat treatment at temperatures 100 °C, 150 °C, and 200 °C for different curing time 2, 4, and 6 h

3.3 Dielectric properties

At room temperature, the dielectric constant vs. RTV-silicon rubber content has been measured at selected frequencies (100 Hz, 1 kHz, and 10 kHz) for composite samples that exposed to heat treatment at temperatures 100 °C, 150 °C, and 200 °C for different curing time 2, 4, and 6 h, as shown in Fig. 4.

Generally, it is found that ϵ' increases with RTV content due to the increase of space charge polarization in the presence of rubber matrix. On the other hand, ϵ' decreases with increasing selected frequency for all samples due to the fact that, as the frequency increases, the dipole polarization effect becomes low and the polarization becomes electronic polarization [38]. Figures 4 shows also ϵ' of rubber ferrite composite decreases with curing time. This happens, because the rubber density and space charge polarization

of NCF in the presence of rubber matrix are reduced as the curing time increases, leading to decrease ϵ' [39].

3.4 AC resistivity

In general, Fig. 5 shows that ρ_{ac} decreases with RTV content for all composite samples. The behavior of resistivity can be explained by considering the porosity and defects of the material. The porosity decreases with increasing RTV content as given from SEM results. The pores and defects act as trapping regions of hopping electrons. Therefore, the reduction in pores and defects with increasing RTV content leads to lower the value of ρ_{ac} . In addition, the electrical conduction contribution from RTV shares in decreasing ρ_{ac} . Figure 5 shows also that the ρ_{ac} decreases with increasing both of the heat treatment temperature and curing time due to the increase of crosslink density of RTV-silicon rubber

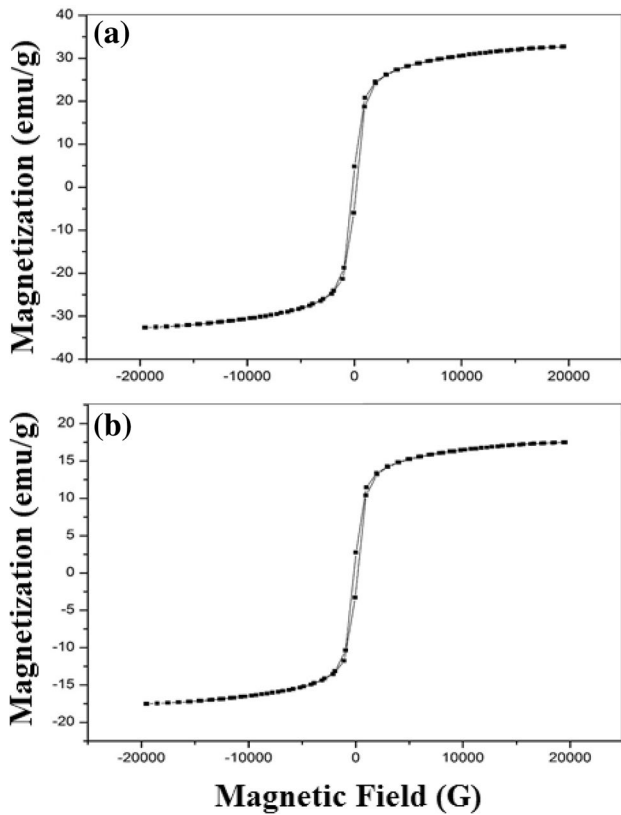


Fig. 6 The hysteresis loop of **a** pure NCF and **b** 0.8 NCF + 1.2 RTV composite

Table 2 Magnetic parameters of pure NCF and 0.8NCF+1.2RTV composite

	Saturation magnetization (M_S) emu/g		H_C (G)	M_r (emu/g)	Squareness
	Experimental	Calculated			
Ferrite	32.68	–	182.5	4.4	0.134
Composite	17.5	13	183.2	1.66	0.140

with increasing both of the heat treatment temperature and curing time [40]. Moreover, ρ_{ac} of all composite samples decrease with increasing selected frequency of the applied field due to the hopping of charge carriers is increased and consequently the ρ_{ac} is decreased.

3.5 Magnetic properties

As shown in Fig. 6, magnetic hysteresis loop for a 0.8 NCF + 1.2 RTV composite sample is demonstrated with $M_S = 11.9$ emu/g, much less than M_S of NCF ($M_S = 32.6$ emu/g), implying the typical weak of

ferrimagnetism in composite sample. In addition, it is clear that the degree of M_S is strongly dependent on NCF content in RTV matrix. The decrease of M_S of composite sample due to incorporation in nonmagnetic matrix (RTV) and the separation between each two particles are increased as it was observed in SEM micrograph of this composite (Fig. 2), leading to lower magnetic exchange interactions for NCF particles. In addition, the RTV matrix is resisted towards the alignment of the magnetic moment of NCF. Furthermore, the diamagnetic contribution from RTV and random dispersion of the NCF particles within the polymeric matrix of RTV cause weak ferromagnetic properties. According to Xiao et al. [41], the saturation magnetization of composite sample $M_C = wM_S$, where M_S is the saturation magnetization for pure ferrite sample and w is the rubber weight fraction. This equation means that the value of M_S of the composite samples can be controlled by the proper selection of the ferrite content within the rubber matrix. The hysteresis loop of composite sample shows a closed with low coercivity, indicating that the composite has low magnetic loss. Applying this equation for our results, we obtain the theoretical value for M_C of rubber ferrite composite that equals 13 emu/g. This value closes to the experimental value 11.9 emu/g. The other magnetic parameters like H_C , M_r , and squareness determined from hysteresis loops are given in Table 2, indicating no significant different values of H_C for two samples and substantial different values of M_r and squareness.

Finally, it is clear that the electrical and magnetic properties are strongly affected RTV content. In addition, the electrical properties can be tailored by heat treatment process at different temperature.

4 Conclusion

RTV-silicon rubber-NCF composites have been synthesized successfully. The RTV content enhances the electrical conductivity and ϵ' . There is a strong correlation between electrical conductivity and curing temperature. Furthermore, the fraction of the RTV-silicon rubber can tailor some magnetic properties like M_S (from 32.68 to 17.5) and M_r (from 4.4 to 1.66) of the NCF–RTV composite. These lead us to conclude that the dielectric and some magnetic properties of these composites can be tailored for various applications such as electromagnetic wave shielding, health care cloth, and magnetic paper by the judicious choice of NCF ferrite and RTV content ratio.

References

1. Y. Gao, Z. Yan, J.L. Gray, X. He, D. Wang, T. Chen, Q. Huang, Y.C. Li, H. Wang, S.H. Kim, T.E. Mallouk, D. Wang, *Nat. Mater.* **18**(4), 384–389 (2019). <https://doi.org/10.1038/s41563-019-0305-8>
2. A.H. El-Sayed, A. Abdelhamed, M.S. Masoud, M.A. Hamad, *Synth. Met.* **245**, 202–208 (2018). <https://doi.org/10.1016/j.synthmet.2018.09.002>
3. A.H. El-Sayed, Y. Hossien, M.A. Hamad, *Eur. Phys. J. Plus* **134**, 415 (2019). <https://doi.org/10.1140/epjp/i2019-12793-8>
4. Y.C. Lu, J. Yu, J. Huang, S. Yu, X. Zeng, R. Sun, C.P. Wong, *Appl. Phys. Lett.* **114**, 233901 (2019). <https://doi.org/10.1063/1.5093968>
5. A.H. El-Sayed, O.M. Hemeda, A. Tawfik, M.A. Hamad, *AIP Adv.* **5**, 107131 (2015). <https://doi.org/10.1063/1.4934790>
6. K.K. Patel, R. Purohit, *Sens. Actuators A* **285**, 17–24 (2019). <https://doi.org/10.1016/j.sna.2018.10.049>
7. S.P. Finner, T. Schilling, P. van der Schoot, *Phys. Rev. Lett.* **122**, 097801 (2019). <https://doi.org/10.1103/PhysRevLett.122.097801>
8. A.H. El-Sayed, F. El-Shamy, Y. Hossien, M.A. Hamad, *J. Supercond. Nov. Magn.* **30**(10), 2927–2931 (2017). <https://doi.org/10.1007/s10948-017-4084-7>
9. M.A. Hamad, A.H. El-Sayed, O.M. Hemeda, A. Tawfik, *Mater. Res. Express* **3**(3), 036104 (2016). <https://doi.org/10.1088/2053-1591/3/3/036104>
10. A.H. El-Sayed, O.M. Hemeda, A. Tawfik, M.A. Hamad, *J. Supercond. Nov. Magn.* **29**(9), 2451–2453 (2016). <https://doi.org/10.1088/2053-1591/3/3/036104>
11. A. Tawfik, O.M. Hemeda, A.H. El-Sayed, M.A. Hamad, *J. Supercond. Nov. Magn.* **29**, 2085 (2016). <https://doi.org/10.1007/s10948-016-3518-y>
12. K.R. Mahmoud, O.M. Hemeda, T. Sharshar, M.A. Hamad, *J. Supercond. Nov. Magn.* **30**, 3143–3154 (2017). <https://doi.org/10.1007/s10948-017-4126-1>
13. O.M. Hemeda, A.H. El-Sayed, A. Tawfik, M.A. Hamad, *Mater. Res. Express* **3**(7), 075302 (2016). <https://doi.org/10.1088/2053-1591/3/7/075302>
14. B.I. Salem, O.M. Hemeda, S.F. Mansour, M.A. Hamad, *Appl. Phys. A* **124**, 621 (2018). <https://doi.org/10.1007/s00339-018-2029-z>
15. O.M. Hemeda, A. Tawfik, A.M. Dorgham, M.A. Hamad, *Appl. Phys. A* **125**(5), 371 (2019). <https://doi.org/10.1007/s00339-019-2666-x>
16. O.M. Hemeda, K.R. Mahmoud, T. Sharshar, M. Elsheshtawy, M.A. Hamad, *J. Magn. Magn. Mater.* **429**, 124 (2017). <https://doi.org/10.1016/j.jmmm.2017.01.018>
17. A.H. El-Sayed, O.M. Hemeda, A. Tawfik, M.A. Hamad, *J. Magn. Magn. Mater.* **402**, 105 (2016). <https://doi.org/10.1016/j.jmmm.2015.11.051>
18. A.H. El-Sayed, O.M. Hemeda, M.A. Hamad, A.M. Mohamed, *J. Supercond. Nov. Magn.* (2019). <https://doi.org/10.1007/s10948-019-05232-3>
19. A.H. El-Sayed, O.M. Hemeda, M.A. Hamad, A.M. Mohamed, *Eur. Phys. J. Plus* **134**, 227 (2019). <https://doi.org/10.1140/epjp/i2019-12751-6>
20. A.H. El-Sayed, M.A. Hamad, *Ph. Transit.* **92**(6), 517–524 (2019). <https://doi.org/10.1080/01411594.2019.1597096>
21. N.D. Sharma, M.K. Verma, N. Choudhary, S. Sharma, D. Singh, *Mater. Sci. Technol.* **35**(4), 448–455 (2019). <https://doi.org/10.1080/02670836.2019.1569836>
22. O.M. Hemeda, M.I. Abdel-Ati, B.I. Salem, A.M.A. Henaish, F.S. El-Sbakhy, *Eur. Phys. J. Plus* **133**, 531 (2018). <https://doi.org/10.1140/epjp/i2018-12346-9>
23. A.R. Chavan, M.V. Shisode, P.G. Undre, K.M. Jadhav, *Appl. Phys. A* **125**, 472 (2019). <https://doi.org/10.1007/s00339-019-2768-5>
24. S.H. Lee, S.J. Yoon, G.J. Lee, H.S. Kim, C.H. Yo, K. Ahn, D.H. Lee, K.H. Kim, *Mater. Chem. Phys.* **61**(2), 147–152 (1999). [https://doi.org/10.1016/S0254-0584\(99\)00136-4](https://doi.org/10.1016/S0254-0584(99)00136-4)
25. Y. Kinemuchi, K. Ishizaka, H. Suematsu, W. Jiang, K. Yatsui, *Thin Solid Films* **407**(1–2), 109–113 (2002). [https://doi.org/10.1016/S0040-6090\(02\)00021-4](https://doi.org/10.1016/S0040-6090(02)00021-4)
26. I.S. Lyubutin, C.R. Lin, S.S. Starchikov, A.O. Baskakov, N.E. Gervits, K.O. Funtov, Y.T. Tseng, W.J. Lee, K.Y. Shih, J.S. Lee, *Inorg. Chem.* **56**(20), 12469–12475 (2017). <https://doi.org/10.1021/acs.inorgchem.7b01935>
27. O.M. Hemeda, D.M. Hemeda, M.Z. Said, *Mech. Time Depend. Mater.* **7**(3–4), 251–268 (2003). <https://doi.org/10.1023/B:MTDM.0000007186.44204.e7>
28. S.M. Patange, S.E. Shirsath, B.G. Toksha, S.S. Jadhav, S.J. Shukla, K.M. Jadhav, *Appl. Phys. A* **95**, 429 (2009). <https://doi.org/10.1142/S021797920905225X>
29. J. Zhang, H. Zhang, H. Wang, F. Chen, Y. Zhao, *Polym. Compos.* **40**(3), 1078–1086 (2019). <https://doi.org/10.1002/pc.24802>
30. S.A. Mansour, M.A. El-Salam, A.H. Moharram, M. Hussein, F.A.M. Al-Agel, *J. Appl. Polym. Sci.* **126**(2), 593–600 (2012). <https://doi.org/10.1002/app.36841>
31. K. Kanamori, *Int. Polym. Sci. Technol.* **13**(2), T-4 (1986)
32. S.A. Seyedmehd, H. Zhang, J. Zhu, *Appl. Surf. Sci.* **258**(7), 2972–2976 (2012). <https://doi.org/10.1016/j.apsusc.2011.11.020>
33. X.L. Gong, X.Z. Zhang, P.Q. Zhang, *Polym. Test.* **24**, 669–676 (2005). <https://doi.org/10.1016/j.polymertesting.2005.03.015>
34. C. Morari, I. Balan, J. Pinteá, E. Chitanu, I. Iordache, *Prog. Electromagn. Res. M* **21**, 93–104 (2011). <https://doi.org/10.2528/PIERM11080406>
35. S.F. Mansour, O.M. Hemeda, S.I. El-Dek, B.I. Salem, *J. Magn. Magn. Mater.* **420**, 7–18 (2016)
36. B. Choudhury, A. Choudhury, *Mater. Chem. Phys.* **131**(3), 666–671 (2012). <https://doi.org/10.1016/j.matchemphys.2011.10.032>
37. O.M. Hemeda, M.A. Hamad, A.M.A. Henaish, *Mater. Res. Express.* **5**(7), 076102 (2018). <https://doi.org/10.1088/2053-1591/aacef3>
38. M.S. Zakerhamidi, A. Ghanadzadeh, M. Moghadam, *Chem. Sci. Trans.* **1**(1), 1–8 (2012). <https://doi.org/10.7598/cst2012.118>
39. K.A. Malini, E.M. Mohammed, S. Sindhu, P. Kurian, M.R. Anantharaman, *Plast. Rubber Comp.* **31**(10), 449–457 (2002). <https://doi.org/10.1179/146580102225006396>
40. X. Wang, Z. Xia, B. Yuan, H. Zhou, Z. Li, N. Chen, *Mater. Des.* **51**, 287–292 (2013). <https://doi.org/10.1016/j.matdes.2013.04.007>
41. Q. Xiao, X. Tan, L. Ji, J. Xue, *Synth. Met.* **157**(18–20), 784–791 (2007). <https://doi.org/10.1016/j.synthmet.2007.08.010>

Publisher's Note Springer Nature remains neutral with regard to jurisdictional claims in published maps and institutional affiliations.